Computer Methods and Programs in Biomedicine 197 (2020) 105739

Contents lists available at ScienceDirect

Computer Methods and Programs in Biomedicine

journal homepage: www.elsevier.com/locate/cmpb

Computational study on electromechanics of electroactive hydrogels for cartilage-tissue repair

Abdul Razzaq Farooqi[a,b,*], Julius Zimmermann[a], Rainer Bader[c,d], Ursula van Rienen[a,d]

[a] Institute of General Electrical Engineering, Faculty of Computer Science and Electrical Engineering, University of Rostock, Albert Einstein Str. 2, Rostock 18059, Germany
[b] Department of Electronic Engineering, Faculty of Engineering, The Islamia University of Bahawalpur, Bahawalpur 63100, Pakistan
[c] Department of Orthopaedics, University Medical Center Rostock, Rostock 18057, Germany
[d] Department Life, Light & Matter, University of Rostock, Rostock 18051, Germany

ARTICLE INFO

Article history:
Received 6 April 2020
Accepted 31 August 2020

Keywords:
Electrical stimulation
Scaffolds
Articular cartilage
Electroactive hydrogels
Finite-element simulation
Multiphysics model

ABSTRACT

Background and Objective: The self-repair capability of articular cartilage is limited because of non-vascularization and low turnover of its extracellular matrix. Regenerating hyaline cartilage remains a significant clinical challenge as most non-surgical and surgical treatments provide only mid-term relief. Eventually, further pain and mobility loss occur for many patients in the long run due to further joint deterioration. Repair of articular cartilage tissue using electroactive scaffolds and biophysical stimuli like electrical and osmotic stimulation may have the potential to heal cartilage defects occurring due to trauma, osteoarthritis, or sport-related injuries. Therefore, the focus of the current study is to present a computational model of electroactive hydrogels for the cartilage-tissue repair as a first step towards an optimized experimental design.

Methods: The multiphysics transport model that mainly includes the Poisson–Nernst–Planck equations and the mechanical equation is used to find the electrical stimulation response of the polyelectrolyte hydrogels. Based upon this, a numerical model on electromechanics of electroactive hydrogels seeded with chondrocytes is presented employing the open-source software FEniCS, which is a Python library for finite-element analysis.

Results: We analyzed the ionic concentrations and electric potential in a hydrogel sample and the cell culture medium, the osmotic pressure created due to ionic concentration variations and the resulting hydrogel displacement. The proposed mathematical model was validated with examples from literature.

Conclusions: The presented model for the electrical and osmotic stimulation of a hydrogel sample can serve as a useful tool for the development and analysis of a cartilaginous scaffold employing electrical stimulation. By analyzing various parameters, we pave the way for future research on a finer scale using open-source software.

1. Introduction

Hyaline cartilage is an avascular, inhomogenous, and multiphasic tissue that is found in articular joints of the body such as the knee and hip [1]. Usually, about 80% of the cartilage tissue is composed of aqueous electrolyte and the remaining ~20% is the solid organic matrix of collagen, chondrocyte cells, proteoglycans, and glycoproteins [2–4]. Based upon shape and alignment of the chondrocytes, and orientation of collagen fibrils, articular hyaline cartilage comprises four zones, namely, calcified, middle, superficial, and transitional [5,6]. The native composition and structure of articular cartilage changes due to osteoarthritis or trauma [7]. Some successes have been made for the regeneration of articular cartilage; however, the complex signal transduction pathways and molecular mechanisms involved in progression of disease and regeneration of the tissue have not been fully understood, which makes it difficult to establish precise proliferation and differentiation methods for chondrogenesis [8,9].

The application of external electric fields is a promising therapeutic approach for healing and regeneration of the biological tissues [10]. The methods to deliver electrical stimulation can be

* Corresponding author.
E-mail address: abdul.farooqi@uni-rostock.de (A.R. Farooqi).

https://doi.org/10.1016/j.cmpb.2020.105739

mainly divided into three main types namely: direct coupling, capacitive coupling, and inductive coupling [11]. In the direct coupling, the electrodes are in contact with the sample, while the other two coupling schemes use electrodes not in direct contact of the sample [12]. Direct coupling can be used either with a direct-current or alternating-current signal, while indirect coupling always works with time-varying, alternating-current signals [13]. Direct methods are widely used because of easy operation [13]. Yet, these methods have certain drawbacks like insufficient biocompatibility of the electrodes, contact to the medium resulting in temperature rise, change in pH, and formation of harmful by-products stemming from redox reactions occurring at the electrodes [14]. On the other hand, capacitive and inductive coupling are biologically more safe as the tissue or sample is not in direct contact with the electrodes [15]. However, this method has the drawback of high voltage requirement to induce an optimal field strength and longer times of operation as compared to the direct coupling [15,16].

Hydrogels have gained much attention for biomedical applications as they possess excellent biocompatibility and biodegradability [17]. They are versatile materials that can encapsulate the seeded cells mimicking the natural structure of the cartilage [18]. In addition, they can be designed in any form, shape, composition, and size and can reversibly swell or deswell upon small biophysical changes in the environment [19].

Polyelectrolyte hydrogels can be tailored to mimic the native cartilage tissue [20]. These hydrogels can either be used as acellular scaffolds for the replacement of injured tissue or as cell-seeded constituents to encourage regeneration and formation of the cartilage tissue [18,21]. Cartilage-tissue repair approaches discussed here involve the cell-seeded hydrogel scaffolds with appropriate biophysical stimuli, like electrical and osmotic stimulation, to create a relatively mature cartilage before its implantation to the defect site *in vivo* [22].

Different biophysical stimuli like mechanical (compression, shear, hydrostatic, osmotic, etc.) [23,24], electrical [25,26], and pulsed electromagnetic fields [27] have been reported to have an effect on the regeneration of articular cartilage. Among these, electrical stimulation (both direct and indirect) has been found to be beneficial for cell-seeded hydrogels in general and cartilage in particular [28]. These studies have mostly been performed with animal and human samples and with living animals, while only a few *in silico* studies are available [29]. Thus, there is a need for *in silico* investigations using electrical stimulation for a complete understanding of the transduction pathways and interaction mechanisms for designing an optimized electrical-stimulation protocol for cartilage-tissue repair [30]. Eventually, successful and validated *in silico* studies will make it possible to perform less biological testings for trying different protocols. Moreover, specialized cues can be designed, i.e., progressing from a trial-and-error approach to well-controlled experiment planning.

Computational or mathematical modeling plays a key role in the improvement of tissue-repair approaches [31]. The development of *in silico* strategies proved to be very helpful in gaining a better understanding of complex biological processes and could thus be used to improve *in vitro* or *in vivo* experiments. Certain hypotheses can be tested *in silico*, although physical implementation would be unacceptable for ethical, technical and safety reasons [32]. Even the study of a simplified mathematical model that ignores many details of biological processes can still be very useful to improve the design of experiments [33,34]. Against this background, we have created *in silico* models as support for the setup of corresponding *in vitro* experiments in order to be able to systematically and theoretically investigate the electrical stimulation of chondrocytes in hydrogel scaffolds over a wide range of parameters.

The application of biophysical stimuli results in the difference of ionic concentrations between the extracellular matrix and the electrolyte solution which creates osmotic pressure and swelling in the cartilage [35]. The electrical stimulation and the resulting osmotic pressure play a significant role in the exchange of essential nutrients and waste products which are ultimately responsible for cartilage growth, stability, and flexibility [24,25]. Variation in calcium ion concentration is the first and fundamental response of the chondrocytes to different biophysical cues (electrical, magnetic, and osmotic etc.), although each type of stimulation has a different mechanism of working [36–38]. Moreover, multiple biophysical cues similar to those experienced by the native cartilage are crucial for tissue-engineering of functional and viable neocartilage [25,26].

The current numerical study focuses on mesoscale, here the scale of the hydrogel scaffold and the surrounding medium. By analyzing the ion distributions, the electrical potential and the osmotic pressure causing the mechanical deformation, we are paving the way for future multiscale studies involving the microscale as well. Moreover, we study the coupling of the electrochemical model to the mechanical model. By this, we eventually estimate the mechanical displacement of the scaffold due to the applied electric stimulus. In Section 2, the tissue engineering approach for cartilage utilizing electrical stimulation has been explained. In Section 3, the mathematical background of the finite-element model for designing electrical-stimulation experiments of electroactive scaffolds has been described. The validated solutions of the numerical model are given in Section 4 while the discussion of results is presented in Section 5.

2. Electroactive scaffolds for cartilage-tissue repair

The electroactive biomaterials are a class of smart materials that allow direct delivery of electrical signals by applying the electric potential. These materials have the advantage of simultaneously providing the stimulus as well as triggering the release of essential therapeutics [39]. Such electroactive hydrogel materials facilitate the researchers in developing new therapeutic approaches for the repair and regeneration of the tissue. The chemical, electrical, and physical properties of these electroactive materials can be tailored for the specific needs of a particular application [40].

Several surgical techniques like microfracture, bone marrow stimulation, osteochondral autograft, and allograft transfer procedures, and some tissue-engineering approaches like autologous chondrocyte implantation and matrix-induced autologous chondrocyte implantation are used for the repair of articular cartilage [41]. Autologous chondrocyte implantation is a two-step tissue engineering procedure, first the chondrocytes from the patient own knee are harvested from a less weight-bearing surface. These cells are then expanded in *in vitro* cultures to increase the cell yield. After a suitable duration, the second surgical procedure is done and the cells are re-implanted at the site of cartilage defect. Matrix-induced autologous chondrocyte implantation is an improved version of the autologous chondrocyte implantation technique which provides the chondrocytes with a supportive scaffold material for the matrix formation and mechanical stability [42]. The main shortcoming of *ex vivo* expansion and cultivation is the de-differentiation of chondrocytes, which makes them lose their chondrogenic phenotype. In order to improve the tissue-engineering approaches for the treatment of articular cartilage, biophysical stimuli like electrical and osmotic stimulation can be used before implantation into the defect site [43]. Eventually, the application of biophysical stimuli results in increased cell proliferation and matrix synthesis while maintaining the chondrogenic phenotype. The complete tissue-engineering approach is illustrated in Fig. 1.

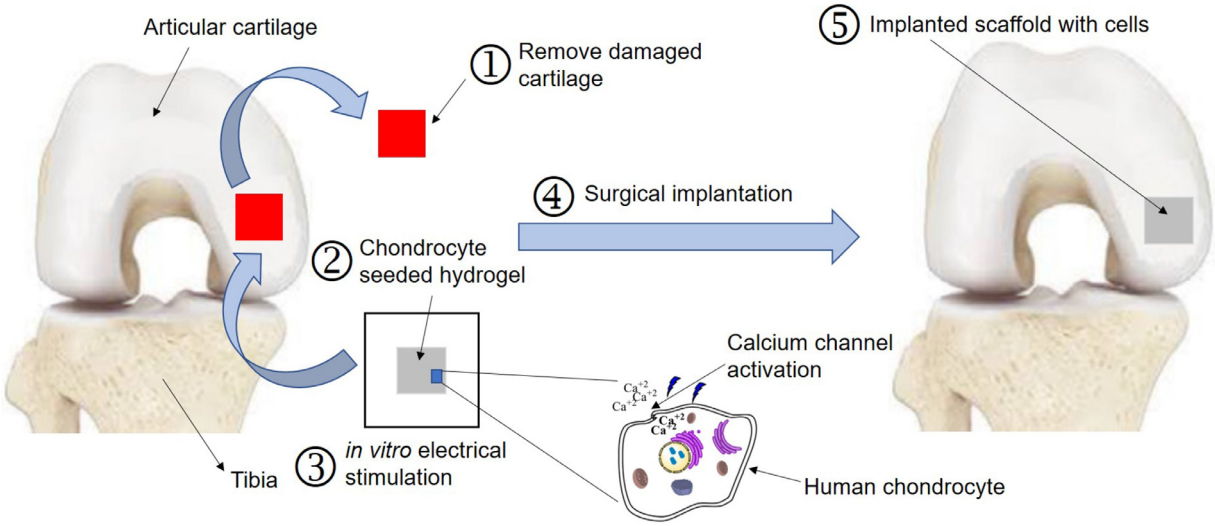

Fig. 1. Different steps involved in the cartilage-tissue repair employing electrical stimulation by transplanting chondrocyte-seeded hydrogel at the defect site. The electric potential stimulates the activity of the Ca^{+2} - calmodulin pathway, followed by the activation of calcineurin and dephosphorylation of a nuclear factor of activated cells (NF-AT). Subsequently, it leads to the expression of genes that are responsible for the growth factors such as transforming growth factor-β (TGF-β) and bone morphogenetic proteins (BMPs). These growth factors are responsible for the repair and regeneration of cartilage. (The figure was adapted from [44].)

Polyelectrolyte hydrogels having fixed anionic groups attached to their polymer chains similar to the native cartilage are suitable for the repair and regeneration of the articular cartilage [45]. Several electroactive hydrogels used for the cartilage tissue repair have been discussed in literature [46–48]. The exact mechanism by which the electrical stimulation affects the tissue growth is still not fully understood. It is hypothesized that as the electrical signal reaches the cell membrane, it changes the transmembrane potential, which leads to the opening of voltage-gated calcium channels [49]. Eventually, the intracellular calcium level increases and thus chondrogenic differentiation of the cell is promoted. The increased intracellular calcium concentration results in activation of calmodulin, followed by the activation of calcineurin, and subsequently dephosphorylation of a nuclear factor of activated cells (NF-AT). Finally, it leads to the expression of genes that are responsible for the growth factors such as transforming growth factor-β (TGF-β) and bone morphogenetic proteins (BMPs) [44,50]. These growth factors are responsible for the repair and regeneration of cartilage [49]. Similarly, the osmotic pressure created due to the applied electric potential activates the transient receptor potential vanilloid (TRPV) channels such as TRPV4. These channels further initiate the transitions of Ca^{+2} [36].

The seeded cells directly experience the electric potential as well as the osmotic pressure generated on either side of the hydrogel scaffold. Thus, the cells are provided with an environment where they are exposed to multiple biophysical stimuli which are required for the tissue-engineering of functional neocartilage [25,26]. As computational models can be used to simulate the various surgical conditions without damaging the specimen, as a first step we have discussed a model for simulation of electroactive hydrogels at the mesoscale which can be extended to study the interactions at the microscale.

3. Mathematical model

As experimental analysis alone cannot fulfill the requirements for novel and complex applications, progress has been made for theoretical modeling of electroactive hydrogels immersed in the electrolyte solution exposed to external electrical stimulation. For example, Doi et al. [51], and Shiga et al. [52,53] investigated the behavior of electrically stimulated hydrogels incorporating the statistical treatment proposed by Flory and Rehner [54–56] and Donnan's equilibrium theory [57]. Similarly, Grimshaw et al. [58,59] using Nernst-Planck and Donnan equations, highlighted the electrically induced swelling in the polyelectrolyte hydrogels. However, these models are not suited for accurately describing the behavior of hydrogels under electrical stimulation.

The biphasic theory was first communicated by Mow et al. [60] for modeling the electromechanical behavior of articular cartilage. Later, this theory was extended to include the ionic phase to give the triphasic [61], quadphasic [62], and then being generalized to a multiphasic theory [63]. Based upon these continuum theories, Gu et al. [64,65] investigated the cartilage tissue under the electro-osmosis phenomenon. But all these theories were more suited for the mechanical stimulation response of the cartilage tissue. The multiphasic theory was used by Zhou et al. [66] and Hon et al. [67] for the modeling of hydrogels immersed in the solution bath. However, this approach had limited applicability since the computational domain was restricted to the hydrogel sample.

Li et al. [68,69] composed a comprehensive multiphasic model based upon mixture theories and added the Poisson–Nernst–Planck equations to study the deformation behavior of hydrogels under the effect of electrical stimulation. The multiphasic model is superior to others since it describes the solvent phase together with the ionic diffusion and deformation of the hydrogel. But it has more unknown independent variables as compared to any other model.

The transport model was first proposed by Grimshaw et al. [58] and later improved by Wallmersperger et al. [70,71] for investigating the polyelectrolyte hydrogel behavior under electrical stimulation. The transport model only describes the ionic concentrations and the hydrogel deformation due to local variations of ion concentrations but neglects water flow. In place of the fluid pressure, the osmotic pressure, arising due to local ionic concentration differences, is considered. Knowing the distribution of ions, the osmotic pressure inside the hydrogel can bebrk calculated.

Both multiphasic and the transport models rely on the nonlinear Poisson–Nernst–Planck equations for describing the ionic concentrations and electrical potential. However, the difference is in the way they couple to the mechanical equilibrium equation and the electrochemical response. The transport model has the advantage of less number of unknowns. Hence, we have used the trans-

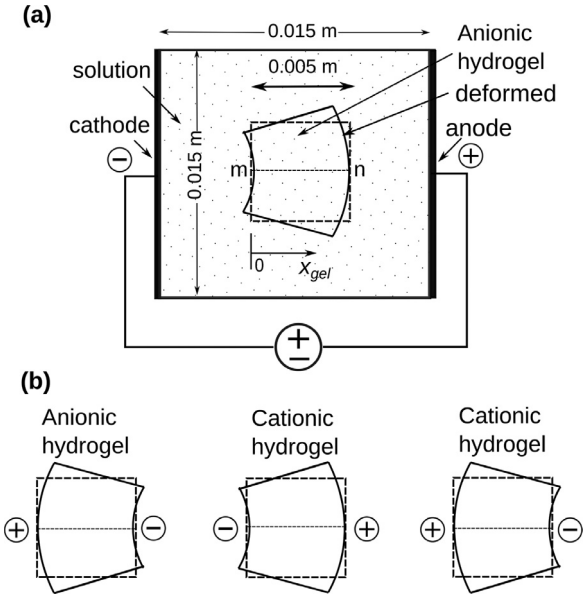

Fig. 2. (a) Sketch of a hydrogel in an electrolyte solution exposed to an external electric field. (b) Further possibilities of deforming the originally square hydrogel depending on the type of hydrogel (anionic or cationic) and the polarity of the applied potential.

port model presented by Wallmersperger et al. [71] for the finite-element simulations and comparison of results.

The electrical stimulation part of the tissue-engineering strategy and the resulting osmotic pressure are of interest here because of their role in the cartilage-tissue repair. The two-dimensional geometry comprising of a square hydrogel sample immersed in solution bath is considered for the finite-element simulations as shown in Fig. 2(a):

$$\Omega = [0.0\,\mathrm{m}, 0.015\,\mathrm{m}] \times [0.0\,\mathrm{m}, 0.015\,\mathrm{m}] \subset \mathbb{R}^2 \tag{1}$$

where Ω represents the computational domain. The representative discretization of the computational domain is shown in Fig. 3. The mesh comprises 3,462,585 elements and 10,387,755 degrees of freedom. Note that it was refined locally such that the maximal edge length was 0.0002 m on either side of the interface. The mesh was refined at both sides of the hydrogel-solution interface, as accuracy is paramount here due to the re-distribution of ionic concentrations on either side of the interface. This refinement was used for all the simulations to obtain good convergence of the solution.

The cells occupy a very small volume (1 - 5%) [5], so they have been ignored for the current mesoscale simulations. In the future, the model can be augmented to study effects on the cellular level as well. The electromechanical behavior of the hydrogel is dictated by the chemical, electrical, and mechanical fields. Two nonlinear, coupled partial differential equations, namely Poisson and Nernst-Planck equations are employed for describing the electrical and chemical fields, respectively, while the momentum equation is used to describe the mechanical field. These equations are described below.

3.1. Poisson equation

The electrical potential is described by the Poisson equation

$$\nabla^2\psi + \frac{F}{\varepsilon_r\varepsilon_o}\left(\sum_{k=1}^{n} z^k c^k + z^f c^f\right) = 0 \tag{2}$$

where ψ is the electric potential, F is Faraday's constant, ε_o is the dielectric constant, ε_r is the relative permittivity of the cell culture medium, $c^{k,f}$ are the ionic concentrations with valence $z^{k,f}$. Note that c^f corresponds to fixed (immobile) ions, while c^k corresponds to mobile ions.

The homogeneous Neumann boundary conditions are considered at the top and bottom surface, whereas non-homogeneous Dirichlet boundary conditions are assumed at the left and right side of the bath solution. Then, Poisson's equation in weak form of the finite element formulation for the two-dimensional case reads [72]

$$\int_\Omega \nabla\psi \cdot \nabla v_\psi \, dA = \frac{F}{\varepsilon_r\varepsilon_o}\int_\Omega \left(z^+c^+ + z^-c^- + z^f c^f\right) v_\psi \, dA \tag{3}$$

where dA represents the two-dimensional differential element for integration over the domain Ω, v_ψ is the test function, whereas two ionic species, i.e., cations '+' and anions '–', have been considered. The test function is considered to vanish, where boundary conditions are imposed.

3.2. Nernst-Planck equation

The total ionic flux $\mathbf{J}^k$ of ion k consists of three components: diffusion flux $(\mathbf{J}^k)_{diff}$ due to the chemical potential gradient of ions,

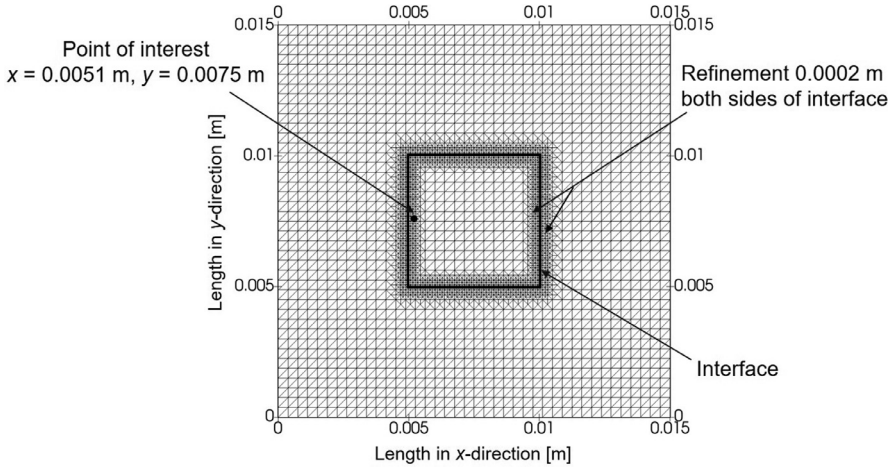

Fig. 3. Discretization of the computational domain with the centrally located hydrogel block and local mesh refinement at the interface between the hydrogel and the electrolyte. In the following analyses we often consider a specific point of interest that we chose at $x = 0.0051$ m and $y = 0.0075$ m, i.e. inside the hydrogel but close to its interface to the electrolyte. On both sides of the interface the mesh was refined such that all edges of the finite elements had a maximal length of 0.0002 m. The mesh was refined at both sides of the hydrogel-solution interface, as accuracy is paramount here due to the re-distribution of ionic concentrations on either side of the interface.

electric transference $(\mathbf{J}^k)_{elect}$ due to the electrical potential gradient, and transfer $(\mathbf{J}^k)_{conv}$ due to the convection, written as [73],

$$(\mathbf{J}^k)_{diff} = -D^k c^k \nabla \mu^k, \tag{4}$$

$$(\mathbf{J}^k)_{elect} = -z^k \mu^k c^k \nabla \psi, \tag{5}$$

$$(\mathbf{J}^k)_{conv} = c^k v \tag{6}$$

where v is the area-averaged fluid velocity, D^k is the diffusivity of the kth ionic species, and μ^k is the ionic mobility. The ionic diffusivity is related to the mobility through the Nernst-Einstein relationship [74] as,

$$\mu^k = \frac{D^k F}{RT}, \tag{7}$$

with T the absolute temperature, and R is the universal gas constant. If the effect of the activity coefficient f^k is explicitly taken into account, the diffusion flux becomes,

$$(\mathbf{J}^k)_{diff} = -D^k\left(\nabla c^k + c^k \nabla \ln f^k\right). \tag{8}$$

The total flux $\mathbf{J}^k$ of the Nernst-Planck equation now reads,

$$\mathbf{J}^k = -\left(D^k \nabla c^k + D^k c^k \nabla \ln f^k + z^k \mu^k c^k \nabla \psi\right) + c^k v. \tag{9}$$

The continuity equation for the ionic flux through the hydrogel scaffold and the cell culture medium is given by,

$$\frac{\partial c^k}{\partial t} + \nabla \cdot \mathbf{J}^k = 0. \tag{10}$$

Under the assumption that neither chemical reactions nor convection occur, the continuity Eq. (10) for the stationary solution becomes [75–77],

$$\nabla \cdot \left(D^k \nabla c^k + z^k \mu^k c^k \nabla \psi\right) = 0. \tag{11}$$

Using the value of μ^k, Eq. (11) becomes,

$$\nabla \cdot \left(D^k \nabla c^k + \frac{z^k F}{RT} D^k c^k \nabla \psi\right) = 0. \tag{12}$$

By multiplication with a test function v_k and integrating over the domain Ω, the weak formulation of Eq. (12) is obtained,

$$D^k \int_\Omega \nabla c^k \cdot \nabla v_k dA + D^k \frac{z^k F}{RT} \int_\Omega c^k \nabla \psi \cdot \nabla v_k dA = 0. \tag{13}$$

In the first step, the Poisson–Nernst–Planck equations are solved numerically using a mixed-function space [78]. This function space consists of second-order Lagrange elements to describe the three scalar functions for anion as well as cation distribution, and the electric potential [79,80]. The given nonlinear problem was solved using the 'NonLinearVariationalSolver' of FEniCS [81] based on Newton's method with the associated solver 'MUMPS' (MUltifrontal Massively Parallel sparse direct Solver) [82]. MUMPS is a direct solver used for the solution of the linear system occurring within Newton's iterations [81]. In the next step, this solution of the Poisson–Nernst–Planck equations is used to find the osmotic pressure and displacement.

3.3. Osmotic pressure and momentum equations

The equation of motion to find the displacement for small deformations is given by [83,84],

$$\rho \frac{\partial^2 \mathbf{u}}{\partial t^2} + f \frac{\partial \mathbf{u}}{\partial t} = \nabla \cdot \sigma + \rho \mathbf{b} \tag{14}$$

where $\mathbf{u}$ is the displacement vector, ρ is the effective density of the gel, f represents the viscous damping between the electrolyte and the polymer fibers, σ is the stress tensor, and $\mathbf{b}$ is the body force. The friction can be neglected due to the absence of body forces and Eq. (14) reduces to,

$$\rho \frac{\partial^2 \mathbf{u}}{\partial t^2} = \nabla \cdot \sigma. \tag{15}$$

Since the redistribution processes of the ionic charges happen at a much lower rate compared to the hydrogel deformation, a quasi-static state can be considered and Eq. (15) becomes,

$$\nabla \cdot \sigma = 0. \tag{16}$$

Further, due to the application of a low potential difference, the electrostatic stress is neglected and Eq. (16) becomes,

$$\nabla \cdot \left(-p_{osm}\mathbf{I} + \lambda_s \mathrm{tr}(\mathbf{S})\mathbf{I} + 2\mu_s \mathbf{S}\right) = 0 \tag{17}$$

where λ_s and μ_s are the Lamé constants, $\mathbf{I}$ is the identity tensor, $\mathbf{S}$ is the strain tensor, $\mathrm{tr}(\mathbf{S})$ is the trace of the strain tensor, and p_{osm} is the osmotic pressure.

The osmotic pressure which depends on the ion concentrations can be calculated from the expression [85],

$$p_{osm} = RT \sum_{k=+,-} \left(c^k_{gel} - c^k_{sol}\right) \tag{18}$$

where c^k_{gel} and c^k_{sol} are the concentrations of the kth ion species in the hydrogel and in the solution next to the hydrogel, respectively. For the steady state one-dimensional simulations, Eq. (17) becomes,

$$(3\lambda_s + 2\mu_s)\frac{\partial^2 u}{\partial x^2} - \frac{\partial p_{osm}}{\partial x} = 0. \tag{19}$$

The linear elastic equation at equilibrium that governs the one-dimensional steady state mechanical deformation of hydrogels [86] is,

$$(3\lambda_s + 2\mu_s)\frac{\partial^2 u}{\partial x^2} - RT\frac{\partial}{\partial x}\left(\sum_{k=+,-}\left(c^k_{gel} - c^k_{sol}\right)\right) = 0. \tag{20}$$

The weak form of Eq. (20) is,

$$(3\lambda_s + 2\mu_s)\left(\int_{\partial\Omega} \frac{\partial u}{\partial n} v_u ds - \int_\Omega \frac{\partial u}{\partial x} \cdot \frac{\partial v_u}{\partial x} dx\right)$$
$$-RT\left(\int_\Omega \frac{\partial}{\partial x}\left(\sum_{k=+,-}\left(c^k_{gel} - c^k_{sol}\right)\right) v_u dx\right) = 0 \tag{21}$$

where v_u is the test function for the displacement and dx denotes the one-dimensional differential element for integration. Applying homogeneous Neumann boundary conditions, Eq. (21) reduces to,

$$-(3\lambda_s + 2\mu_s)\int_\Omega \frac{\partial u}{\partial x} \cdot \frac{\partial v_u}{\partial x} dx = RT\left(\int_\Omega \frac{\partial}{\partial x}\left(\sum_{k=+,-}\left(c^k_{gel} - c^k_{sol}\right)\right) v_u dx\right). \tag{22}$$

The complete simulation scheme is shown in Fig. 4.

4. Results

In order to validate the proposed simulation scheme, Eqs. (3), (13), and (22) were solved numerically by means of the simulation scheme described in Fig. 4. The initial concentration of fixed negative ions c^f was maintained at 8 mM. The other quantities for the simulation are described in Table 1. The displacement of the hydrogel obtained as the last step of the model was compared with the displacement result of multiphasic theory from the study reported by Li et al. [87]. It is evident from Fig. 5 that both results are in good agreement which verifies our modeling approach using the open-source software. In the following, the model is explained in detail making comparisons to the examples from literature.

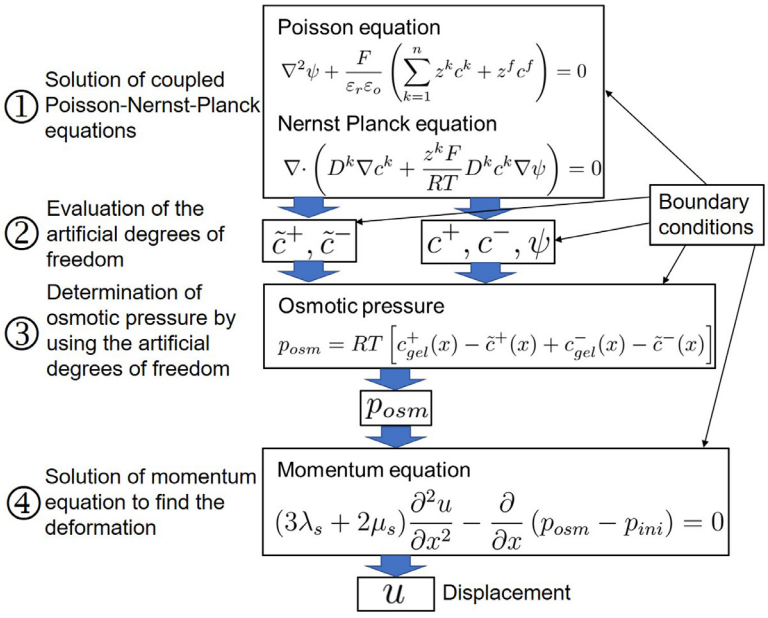

Fig. 4. Simulation flow chart of the model.

Table 1
Quantities used for simulations in accordance with [88].

Parameter	Value
Ionic mobility μ^k	3.9607 × 10^{-6} m^2 s^{-1} V^{-1}
Ionic diffusion coefficient D^k	1.0 × 10^{-7} m^2 s^{-1}
Gas constant R	8.3143 J mol^{-1} K^{-1}
Temperature T	298.0 K
Relative permittivity ε_r	80.0
Vacuum permittivity ε_o	8.854 × 10^{-12} A sV^{-1} m^{-1}
Faraday constant F	9.6487 C mol^{-1}
Ionic valence z^k	± 1.0
Fixed charge valence z^f	- 1.0
Lamé coefficient $3\lambda + 2\mu$	1.2 × 10^5 Pa
External electric potential ψ	± 100 mV
Hydrogel dimensions	0.005 × 0.005 m^2
Solution bath dimensions	0.015 × 0.015 m^2

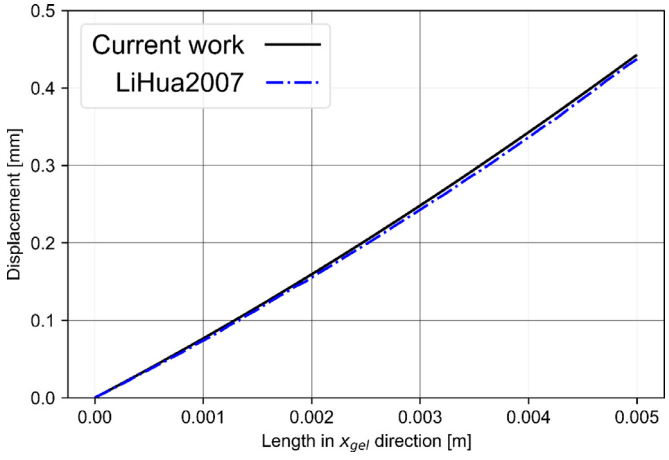

Fig. 5. Comparison of values of horizontal displacement as a function of the coordinate x_{gel} within the hydrogel. The blue dash-point line shows the values calculated by Li et al. [87] with the multiphase theory and taken from this publication. The black solid line shows the results from our simulation model according to Fig. 4 (last step of the simulation procedure). Although these are two different mathematical approaches, the agreement of the results can be regarded as very good.

4.1. Chemical stimulation

The behavior of the hydrogel sample under chemical stimulation is considered in this section. The hydrogel sample with initial concentration of fixed negative charges $c^f = 2$ mM = 2 mmol/l = 2 mol/m^3 was placed in between the electrodes in a cell culture medium with concentration of 1 mM as shown in Fig. 2(a). For the numerical simulation, a concentration of 1 mM was assumed for both anions and cations as a boundary condition at the boundaries of that part of the computational area which is assigned to the electrolyte solution. The difference of ionic concentrations between the solution and the hydrogel compels the mobile ions to redistribute in the whole region for maintaining the electroneutrality condition. The ionic concentration difference results in a negative step in the electric potential, as displayed in Fig. 6(f).

The concentration of ions in the hydrogel at Donnan equilibrium can be evaluated using [62,89]

$$c^{\pm}_{\text{gel}} = \frac{1}{2}\left(\mp c^f + \sqrt{[c^f]^2 + 4[c^{\pm}_{\text{sol}}]^2}\right). \tag{23}$$

The corresponding Donnan potential can be found by using the relation [90–92],

$$\Delta\phi = \frac{RT}{z^k F}\ln\left(\frac{c^k_{\text{gel}}}{c^k_{\text{sol}}}\right). \tag{24}$$

Using Eqs. (23) and (24), the concentration of anions, cations, and the Donnan potential were found to be 0.4142 mM, 2.4142 mM, and -22.2522 mV, respectively. Similar results were obtained by numerically solving the Eqs. (3) and (13) which also agree to the results reported by Wallmersperger et al. [71]. The parameters used are listed in Table 1 and the simulation results are shown in Fig. 6.

4.2. Electrical stimulation

The chemo-electrical behavior of the hydrogel sample under electrical stimulation is considered in this section. For the two-dimensional numerical simulation, the concentration of negative fixed charges for the hydrogel was set to $c^f = 2$ mM. For the concentration of free Na^+ and Cl^- ions in the solution, the concentrations at the electrodes were set to $c^+ = c^- = 1$ mM using the

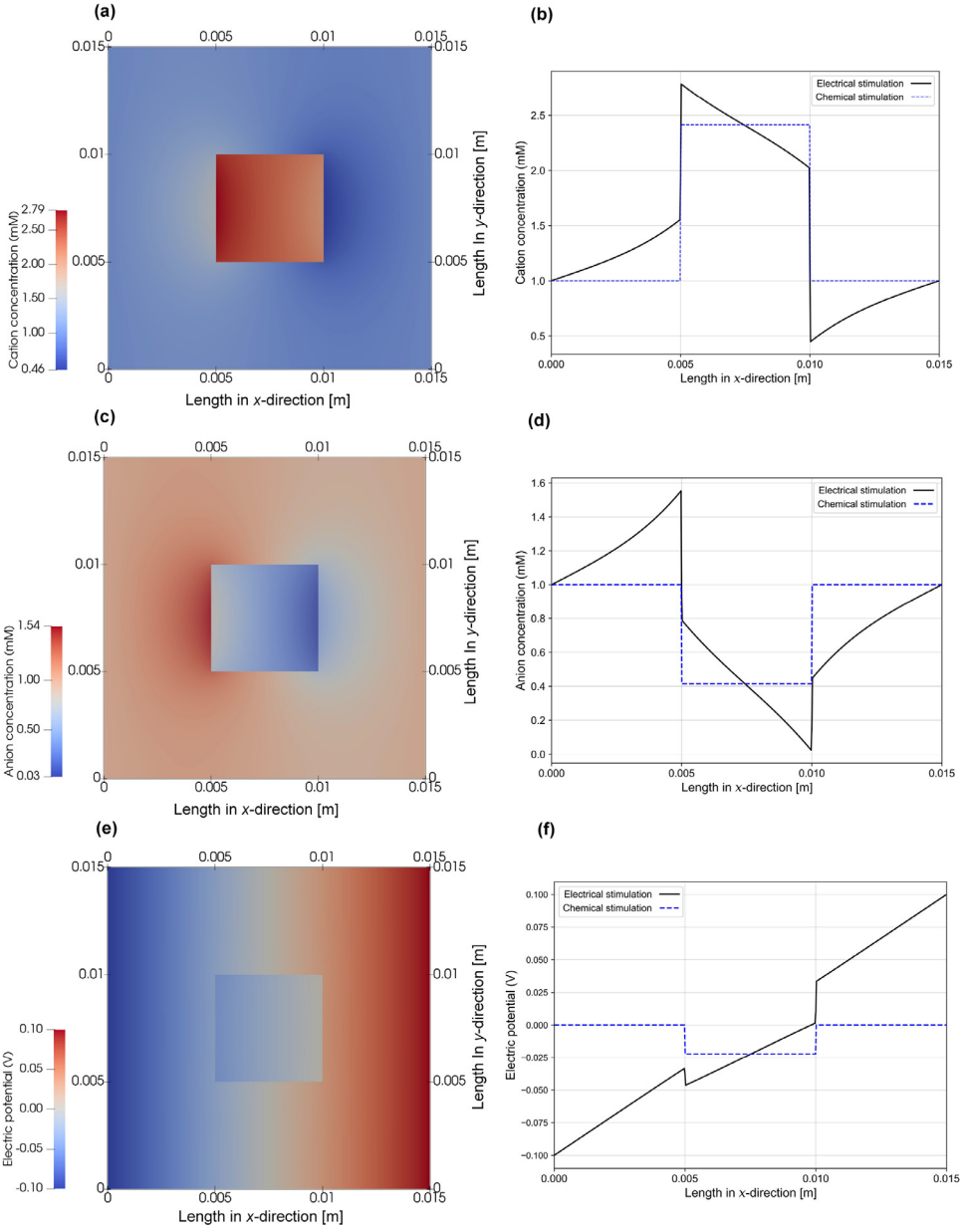

Fig. 6. Ionic concentrations and electric potential distributions for the hydrogel sample immersed in the solution bath. Cation distribution: (a) under two-dimensional electrical stimulation, (b) Comparison under chemical and electrical stimulation. Anion distribution: (c) under two-dimensional electrical stimulation, (d) Comparison under chemical and electrical stimulation. Electric potential distribution: (e) under two-dimensional electrical stimulation, (f) Comparison under chemical stimulation and electrical stimulation. One-dimensional values of the quantities are plotted at $y = 0.0075$ m versus the x-direction.

Dirichlet boundary conditions. A constant electric potential of -100 mV was prescribed directly at the cathode and + +100 mV at the anode. As initial conditions for numerical simulation, the results of the chemical stimulation, i.e., without applied external electric field were used. Other quantities used for the numerical solution were identical to those for the chemical stimulation, as given in Table 1. The presented numerical results for the chemical and electrical stimulation are in accordance to the numerical simulation results reported by Wallmersperger et al. [71] except that here the value of applied electric potential is ± 100 mV instead of ± 50 mV. The presented results also agree qualitatively to the experimental results reported by Gülch et al. [93].

The computation time for the two-dimensional Poisson–Nernst–Planck equations under electrical stimulation was ~ 10 min with 10,387,755 degrees of freedom. The appropriate number of degrees of freedom was chosen upon convergence analysis (Section 4.4). Concentrations as well as electric potential were found to have a relative error less than 0.1% (Fig. 10). Large number of the degrees of freedom is necessary as the coupled Poisson–Nernst–Planck equations are nonlinear, and the solution tends to become unstable at the hydrogel-solution interface by the occurrence of nonphysical negative ionic concentrations. The simulations were performed on a computer with Intel(R) Xeon(R) E5-2687W v4 CPU @ 3.00 GHz with 256 GB RAM without using parallelization. The Python scripts related to the current study can be accessed through an online repository (https://github.com/arfarooqi/Electromechanics_hydrogels).

The electric field distribution for the hydrogel sample immersed in the solution bath can be found using,

$$\mathbf{E} = -\nabla\psi. \tag{25}$$

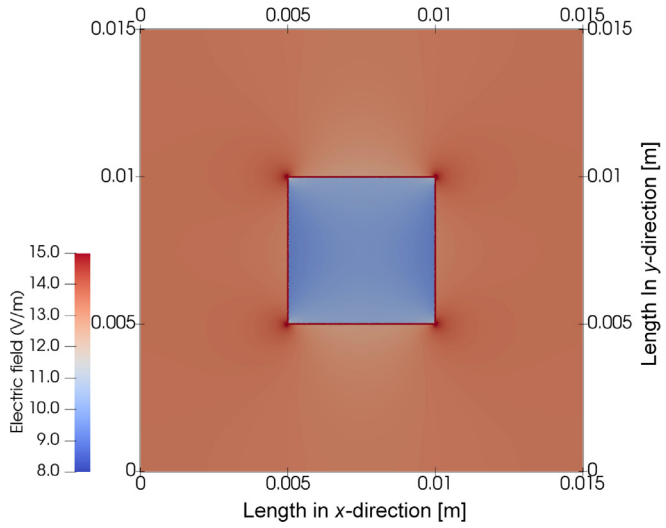

Fig. 7. Distribution of the electric field strength in the hydrogel and its surrounding solution. The color coding shows the local distribution of the electric field strength taking values of 8 - 15 V/m. The increase of the field at the sharp corners of the square hydrogel is clearly visible.

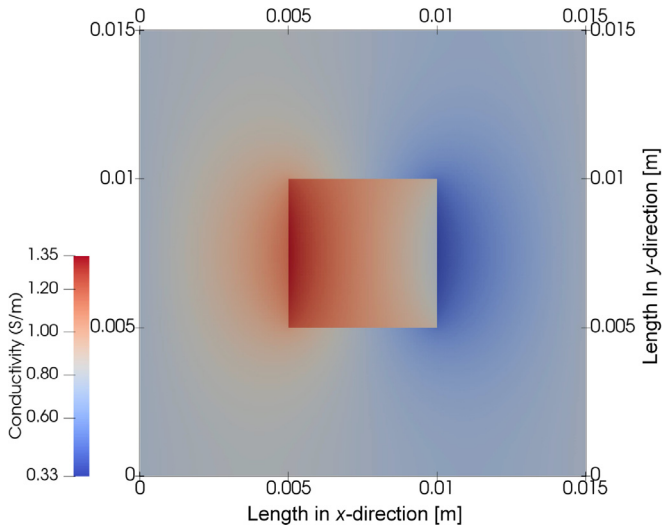

Fig. 8. Values of electrical conductivity for the hydrogel sample immersed in the electrolyte solution, calculated using the Nernst-Einstein relationship from Eq. (7). The color coding refers to the conductivity values of 0.33 - 1.75 S/m.

The electric field inside the hydrogel is mostly homogeneous as shown in Fig. 7. There are inhomogeneities at the sharp corners of the hydrogel sample due to the well-known edge effect of the electric field at sharp tips and corners. From Eq. (2), the electric field depends on ionic concentrations, fixed charge density, and the permittivity of the medium. The field distribution can further be optimized by varying these parameters as per requirement. The chosen value for the electrical potential was used to investigate the suitability and validation of our proposed simulation model for cartilage tissue repair in implementation in the open source software FEniCS as shown in Fig. 4. It is straightforward to perform the simulations for other potential values. Our future studies using this model will aim to use experimental data as they become available. In any case, the resulting electric field strengths in the range of a few V/m correspond to the values usually applied in experiments [94,95].

The electrical conductivity κ of the experimental setup is not constant but can be correlated to the concentration of ions and their respective diffusivities by using the Nernst-Einstein relation of Eq. (7) as,

$$\kappa = \frac{F^2}{RT}\left(\sum_{k=1}^{n}(z^k)^2 D^k c^k\right). \tag{26}$$

The electrical conductivity is plotted in Fig. 8. The conductivity of the hydrogel depends upon its fixed ionic groups, the concentration of the solution in which it is immersed, and diffusivity of the ionic species. The Poisson–Nernst–Planck system of equations yields a more accurate description of the electrical stimulation than the electrostatic equation, where the conductivity would enter as a fixed, homogeneous value for each domain. By taking into account the ion motion, the Poisson–Nernst–Planck system allows for local changes of the conductivity.

4.3. Osmotic stimulation and displacement

This osmotic pressure created due to the difference of ionic concentrations compels the hydrogel to take up solvent, resulting in hydrogel swelling. The osmotic pressure can be associated with a strain imposed on the mechanical field Eq. (17). The method reported by Wallmersperger et al. [96] was used to find the osmotic pressure difference. As evident from Fig. 9(a), the osmotic pressure varies in the entire hydrogel sample and should be determined locally. To attain this, information about the non-local values of the corresponding ionic concentrations in the nearby solution is required. Thus, two artificial degrees of freedom are introduced which interpolate the ionic concentrations of mobile ions at the hydrogel-solution interface into the hydrogel. These degrees of freedom are represented by $\tilde{c}^+(x)$ and $\tilde{c}^-(x)$ for cations and anions, respectively. More specifically, the local value of the one-dimensional osmotic pressure difference as function of x can be calculated using Eq. (18) as

$$p_{osm} = RT\left[c^+_{gel}(x) - \tilde{c}^+(x) + c^-_{gel}(x) - \tilde{c}^-(x)\right]. \tag{27}$$

The osmotic pressure evaluated for the hydrogel is illustrated in Fig. 9(b) which serves as input for the mechanical field Eq. (20).

It is not reasonable to start the solution of the system from the complete dry condition. Thus, an initial osmotic pressure is introduced into the mechanical equation. This initial value can be found using the osmotic pressure created due to the chemical stimulation as

$$p_{ini} = RT\left(c^+_{gel} - c^+ + c^-_{gel} - c^-\right). \tag{28}$$

For the current one-dimensional case, the initial osmotic pressure using Eq. (18) is found to be 2.052 kPa and Eq. (20) can be written as

$$(3\lambda_s + 2\mu_s)\frac{\partial^2 u}{\partial x^2} - \frac{\partial}{\partial x}(p_{osm} - p_{ini}) = 0, \tag{29}$$

where p_{osm} is determined by the Eq. (27). The weak form of Eq. (29) is,

$$-(3\lambda_s + 2\mu_s)\int_\Omega \frac{\partial u}{\partial x}\cdot\frac{\partial v_u}{\partial x}dx = RT\left(\int_\Omega \frac{\partial p_{osm}}{\partial x}v_u dx - \int_\Omega \frac{\partial p_{ini}}{\partial x}v_u dx\right). \tag{30}$$

Solving Eq. (30) numerically gives the hydrogel displacement as illustrated in Fig. 9(c) which is in agreement to the numerical result reported by Li et al. [88]. The displacement u was measured at the edge point n of the one-dimensional computational domain between the edge points m and n in the direction of hydrogel thickness along symmetric x-axis as depicted in Fig. 2(a). In Fig. 5, our modeling approach using the open-source software was initially validated while in Fig. 9 the model has been further explained in detail making comparisons to the examples from literature.

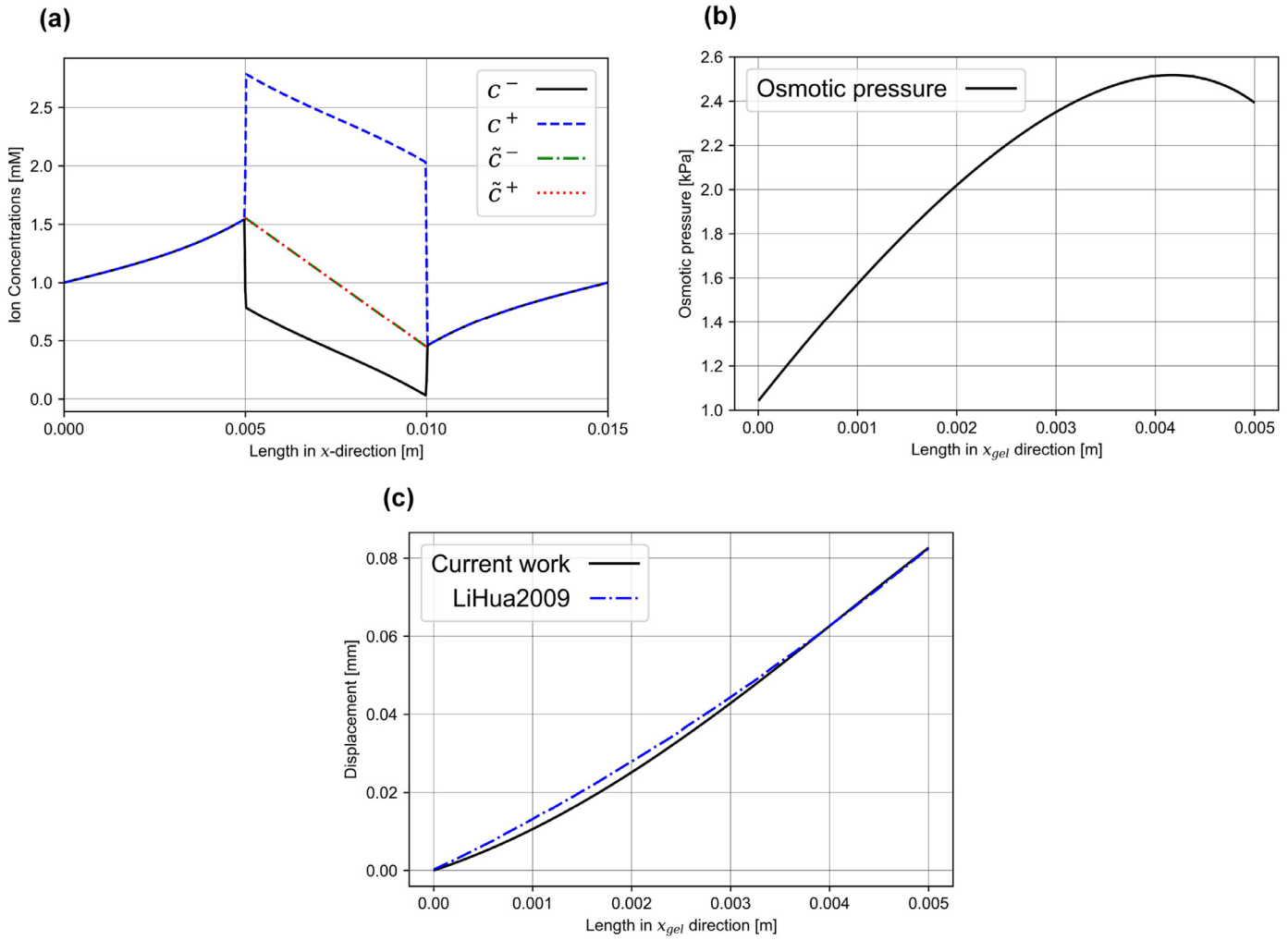

Fig. 9. (a) Ion concentration in the hydrogel and its surrounding electrolyte solution as a function of x at $y = 0.0075$ m to evaluate the osmotic pressure difference as obtained for the chemo-electric coupling scheme under electrical stimulation. Shown are the functional curves for cations (blue dashed line), anions (solid black line) and the corresponding artificial degrees of freedom (red dotted line and green dash-point line), which interpolate the concentration of mobile ions at the hydrogel-electrolyte interface. All curves differ only in the hydrogel. (b) Osmotic pressure as a function the coordinate x_{gel} within the hydrogel due to the variation in ion concentration shown in (a). Note the different abscissas in (a) and (b). (c) Comparison of values of horizontal displacement as a function of the coordinate x_{gel} within the hydrogel. The blue dash-point line shows the values reported by Li et al. [88] with the multiphase theory and taken from this publication. The black solid line shows the results from our simulation model according to Fig. 4 using Eq. (30). Although these are two different mathematical approaches, the agreement of the results can be regarded as very good.

4.4. Convergence analysis

In order to demonstrate convergence of our finite element simulations, the relative error was evaluated for the ionic concentrations and the electric potential at a representative point ($x = 0.0051$ m, $y = 0.0075$ m) just inside the hydrogel, while refining the mesh. A local mesh refinement of 0.0002 m was used on both sides of the interface as shown in Fig. 3 because it is the region where the solution tends to become unstable. The convergence study was initiated from one refinement cycle in a distance of 0.0002 m on either side of the interface and ended at the sixth cycle while keeping the mesh in the remaining solution domain constant in each refinement cycle. The relative error is found using the relation

$$\text{relative error} := \frac{\|u_i - u_{i-1}\|}{\|u_i\|} \tag{31}$$

where u_i and u_{i-1} are the current and previous values, respectively. The relative error in the ionic concentrations of anions, cations, and electric potential distribution at a representative point ($x = 0.0051$ m, $y = 0.0075$ m) is plotted against the degrees of freedom as given in Fig. 10. Expectedly the relative error reduces as the degrees of freedom increase. This happens in two stages: after a first, steeper descend with the order of approx. 4, the descend reduces to the order of approx. 1 while approaching zero. Clearly, the relative error for anions, cations and electric potential tends to zero if the mesh consists of more than 10 million degrees of freedom. The global convergence was checked as well by computing the L^2 error using the relation

$$L^2 \text{ error} = \|u_i - u_{i-1}\| = \sqrt{\int_\Omega (u_i - u_{i-1})^2 dA}. \tag{32}$$

A steadily converging solution is observed as it is evident from Fig. 11. The global error for the ionic concentrations of anions, cations, and electric potential distribution converges with approximately $\mathcal{O}\left(n^{-1/3}\right)$ for the adaptive refinement scheme.

5. Discussion

Applying electrical stimulation to the hydrogel sample immersed in the solution bath causes the ions to redistribute in the hydrogel and solution. It is because of a higher potential difference created on one side of the hydrogel and a lower on the other side.

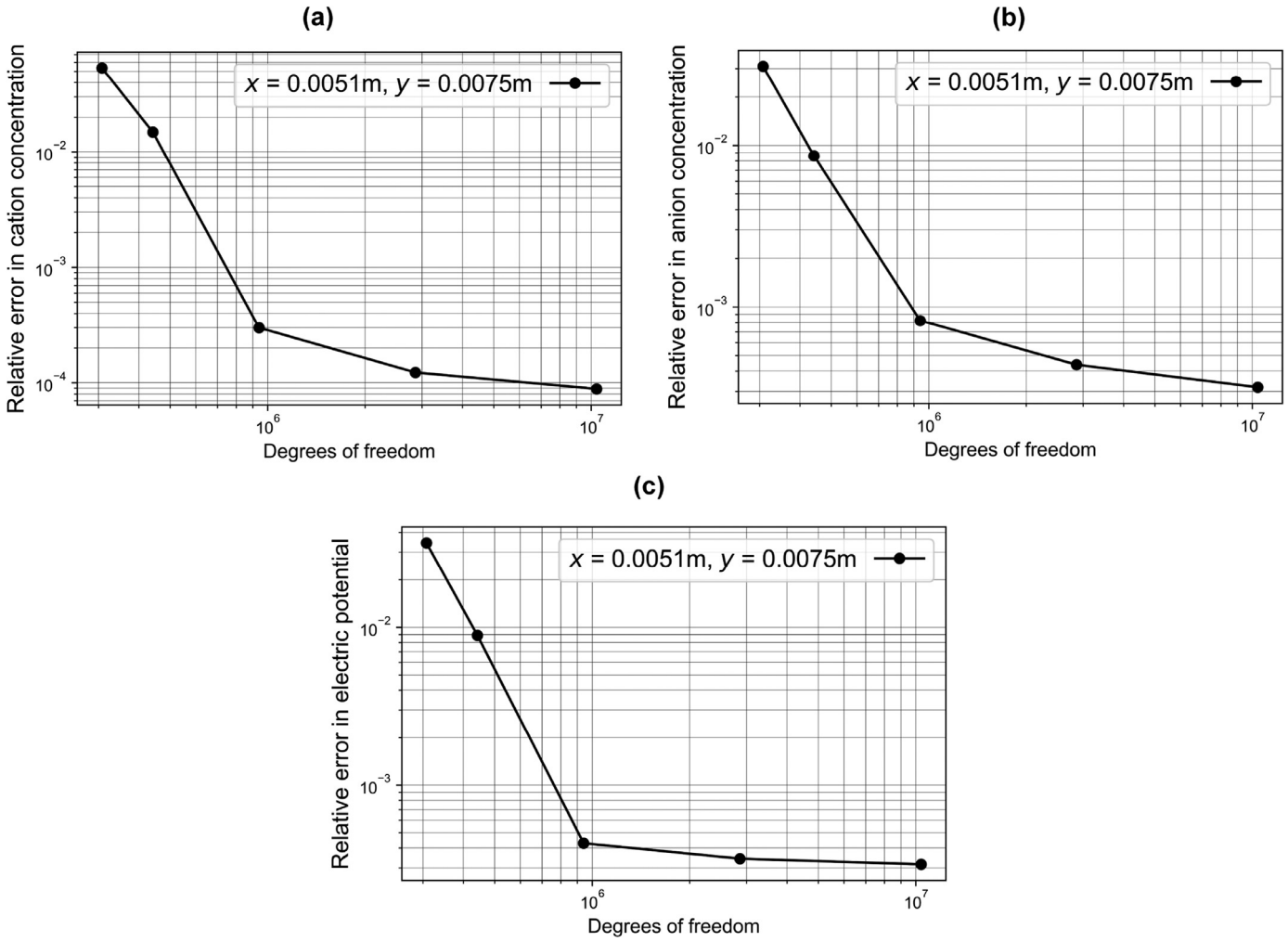

Fig. 10. Relative error according to Eq. (31) computed at the point of interest shown in Fig. 3: (a) Cation concentration, (b) Anion concentration, (c) Electric potential. Up to one million degrees of freedom, the relative error decreases significantly in each case. After that the convergence rate decreases. At 10 million degrees of freedom a sufficiently small relative error is reached.

Due to the fixed charges attached to the polymers of the hydrogel, the diffusion process causes ionic concentration differences between the exterior solution and the interior hydrogel. So, we get an increased swelling on one side whereas a reduced swelling takes place on the other side. Accordingly, the ionic concentration difference results in an osmotic pressure which causes the shrinking or swelling of the hydrogel. The deformation of the hydrogel induces reorganization of the diffused ions and bound anionic charges resulting in modified ionic concentration differences and the hydrogel bends. This mechanism continues till the increase in mechanical energy equalizes the decrease in free energy of the system.

The bending direction depends on the type of hydrogel (anionic or cationic fixed charge groups) and the polarity of the applied electrical stimulation. With anionic hydrogels, there is an increase in the potential difference or an additional swelling on the side facing the anode and a decrease in the potential difference or shrinkage on the opposite side. This leads to a bend in the direction of the cathode as shown in Fig. 2(a). For cationic hydrogels, however, the reverse effect occurs, i.e., they bend towards the anode. Various possible scenarios depending upon the type of hydrogel used and polarity of the applied potential are schematically illustrated in Fig. 2(b).

Various approaches for cartilage-tissue repair were experimentally performed using electrical [47,97–100] and osmotic [24,101,102] stimulation but appropriate computational models have still not been presented. Keeping this in mind, we have proposed a mathematical model to comprehend the experimental procedures for the engineering of cartilage tissue using electrical and osmotic stimulation. The proposed model was then solved numerically using the open-source platform FEniCS. A similar setup was also experimentally studied by Lim et al. [103] using human mesenchymal stem cells under electric stimulation for cell viability, proliferation, and chondrogenic differentiation. These experimental investigations can be enhanced by numerical simulations to study the chondrocyte-hydrogel interactions and transduction pathways at the microscale.

5.1. Limitations

The numerical model presented here has following limitations. First, the cells have not been included explicitly. Nevertheless, the model has the capability to include the cellular inclusions as well. Second, there is an abrupt change in values at the hydrogel-solution interface which is not realistic. This could be addressed by using the model proposed by Li et al. [68] but it is characterized by a higher number of unknowns. Third, the current numerical method is computationally rather expensive due to high number of degrees of freedom. The numerical method can be further optimized for example by using the physics-based refinement [104] instead of the currently used local mesh refinement.

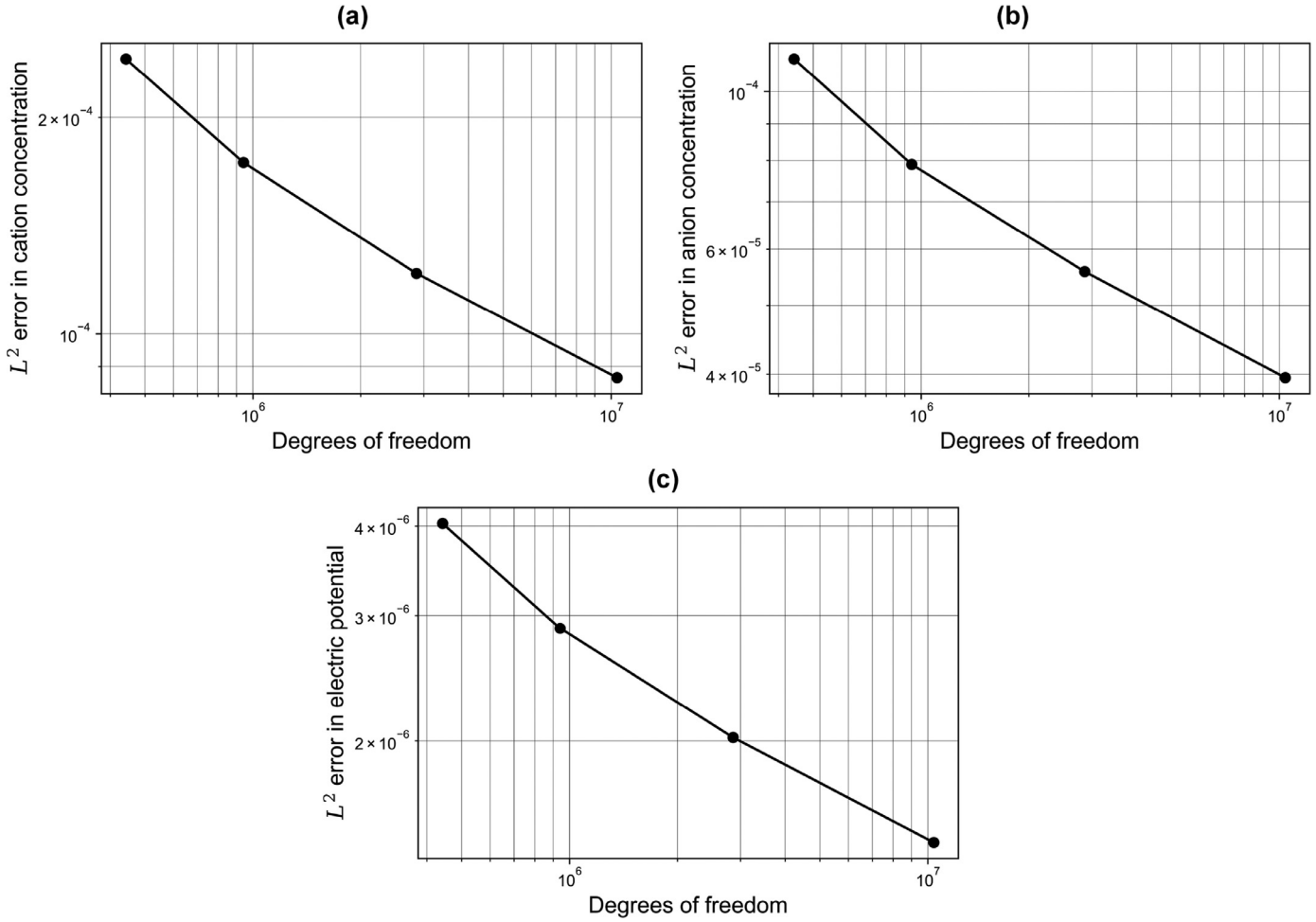

Fig. 11. Global convergence by evaluating L^2 error according to Eq. (32) computed at the interest shown in Fig. 3: **(a)** Cation concentration, **(b)** Anion concentration, **(c)** Electric potential. In each case the global error for the ionic concentrations of anions, cations, and electric potential distribution converges with approximately $\mathcal{O}\left(n^{-1/3}\right)$ for the adaptive refinement scheme.

6. Conclusions

The establishment of robust and reproducible computer simulations takes on a pivotal role in complementing novel experimental techniques to understand the state of health and progress of diseases and thus aid in their diagnosis and treatment. Computational models can be used to simulate therapeutic outcomes, so that fewer *in vitro* and *in vivo* studies are required [105,106]. In our current study, the open-source software FEniCS has been used for the finite-element simulations of electroactive hydrogel samples in a bath solution under electrical and osmotic stimulation. However, modeling the behavior of such hydrogel samples under biophysical stimulation is challenging due to nonlinear coupled equations involving the chemical, electrical, and mechanical multiphysics. Such models have been numerically simulated using custom programs developed in individual workgroups that are usually not available publicly. Thus, we have performed the simulations of electroactive hydrogels [107,108] using FEniCS in the context of the cartilage-tissue repair. The proposed model was validated by comparison with data from the literature. Furthermore, its application as a model for the tissue engineering using biophysical stimulation is explained in detail.

The proposed model has the capability to include other stimuli like pH, mechanical stress, oxygen, and glucose, or a combination of two or more stimuli. In addition, it can also be used to study drug delivery mechanisms. Moreover, the cellular interactions of chondrocytes with porous hydrogel scaffolds can be modeled at the microscale by the addition of appropriate equations. Thus, the proposed model is a step forward in establishing comprehensive simulation models for the engineering of optimized cartilage scaffolds.

Funding

The work is funded by the Higher Education Commission (HEC), Pakistan through a doctoral scholarship in collaboration with German Academic Exchange Service (DAAD); and the Deutsche Forschungsgemeinschaft (DFG, German Research Foundation) - SFB-1270/1 - 299150580.

Declaration of Competing Interest

The authors declare that they have no known competing financial interests or personal relationships that could have appeared to influence the work reported in this paper.

Acknowledgments

The authors would like to thank Dr. Yogesh Bansod for fruitful discussions regarding the mechanical concepts and Dr. Jonathan Dawson for his critical reading of the manuscript and valuable comments.

References

[1] Y. Krishnan, A.J. Grodzinsky, Cartilage diseases, Matrix Biol. 71-72 (2018) 51–69, doi:10.1016/j.matbio.2018.05.005.

[2] V.C. Mow, A. Ratcliffe, A. Robin Poole, Cartilage and diarthrodial joints as paradigms for hierarchical materials and structures, Biomaterials 13 (1992) 67–97, doi:10.1016/0142-9612(92)90001-5.

[3] A.J.S. Fox, A. Bedi, S.A. Rodeo, The basic science of articular cartilage: structure, composition, and function, Sports Health 1 (2009) 461–468, doi:10.1177/1941738109350438.

[4] V.C. Mow, C.C. Wang, C.T. Hung, The extracellular matrix, interstitial fluid and ions as a mechanical signal transducer in articular cartilage, Osteoarthr. Cartil. 7 (1999) 41–58, doi:10.1053/joca.1998.0161.

[5] A.M. Bhosale, J.B. Richardson, Articular cartilage: Structure, injuries and review of management, Br. Med. Bull. 87 (2008) 77–95, doi:10.1093/bmb/ldn025.

[6] F. Taraballi, G. Bauza, P. McCulloch, J. Harris, E. Tasciotti, Concise review: biomimetic functionalization of biomaterials to stimulate the endogenous healing process of cartilage and bone tissue, Stem Cells Transl. Med. 6 (2017) 2186–2196, doi:10.1002/sctm.17-0181.

[7] N.P. Cohen, R.J. Foster, V.C. Mow, Composition and dynamics of articular cartilage: structure, function, and maintaining healthy state, J. Orthop. Sport. Phys. Ther. 28 (1998) 203–215, doi:10.2519/jospt.1998.28.4.203.

[8] H.J. Samvelyan, D. Hughes, C. Stevens, K.A. Staines, Models of osteoarthritis: relevance and new insights, Calcif. Tissue Int. 2020, Accepted (2020), doi:10.1007/s00223-020-00670-x.

[9] B. Johnstone, M.J. Stoddart, G.I. Im, Multi-disciplinary approaches for cell-based cartilage regeneration, J. Orthop. Res. 38 (2020) 463–472, doi:10.1002/jor.24458.

[10] R.H.W. Funk, T. Monsees, N. Özkucur, Electromagnetic effects - from cell biology to medicine, Prog. Histochem. Cytochem. 43 (2009) 177–264, doi:10.1016/j.proghi.2008.07.001.

[11] R. Balint, N.J. Cassidy, S.H. Cartmell, Electrical stimulation: a novel tool for tissue engineering, Tissue Eng. Part B Rev. 19 (2013) 48–57, doi:10.1089/ten.TEB.2012.0183.

[12] G. Thrivikraman, S.K. Boda, B. Basu, Unraveling the mechanistic effects of electric field stimulation towards directing stem cell fate and function: a tissue engineering perspective, Biomaterials 150 (2018) 60–86, doi:10.1016/j.biomaterials.2017.10.003.

[13] L.P. da Silva, S.C. Kundu, R.L. Reis, V.M. Correlo, Electric phenomenon: a disregarded tool in tissue engineering and regenerative medicine, Trends Biotechnol. 38 (2020) 24–49, doi:10.1016/j.tibtech.2019.07.002.

[14] D.R. Merrill, M. Bikson, J.G. Jefferys, Electrical stimulation of excitable tissue: design of efficacious and safe protocols, J. Neurosci. Methods 141 (2005) 171–198, doi:10.1016/j.jneumeth.2004.10.020.

[15] C. Chen, X. Bai, Y. Ding, I.-s. Lee, Electrical stimulation as a novel tool for regulating cell behavior in tissue engineering, Biomater. Res. 23 (2019) 25, doi:10.1186/s40824-019-0176-8.

[16] S. Meng, M. Rouabhia, Z. Zhang, Electrical stimulation in tissue regeneration, in: G.D. Gargiulo, A. McEwan (Eds.), Applied Biomedical Engineering, IntechOpen, Rijeka, 2011, pp. 37–62, doi:10.5772/18874.

[17] A.S. Hoffman, Hydrogels for biomedical applications, Adv. Drug Deliv. Rev. 64 (2012) 18–23, doi:10.1016/j.addr.2012.09.010.

[18] S. Fuchs, K. Shariati, M. Ma, Specialty tough hydrogels and their biomedical applications, Adv. Healthc. Mater. 9 (2020) 1901396, doi:10.1002/adhm.201901396.

[19] L. Hu, Y. Wan, Q. Zhang, M.J. Serpe, Harnessing the power of stimuli-responsive polymers for actuation, Adv. Funct. Mater. 30 (2020) 1903471, doi:10.1002/adfm.201903471.

[20] E.A. Aisenbrey, S.J. Bryant, The role of chondroitin sulfate in regulating hypertrophy during MSC chondrogenesis in a cartilage mimetic hydrogel under dynamic loading, Biomaterials 190-191 (2019) 51–62, doi:10.1016/j.biomaterials.2018.10.028.

[21] S.G. Walter, R. Ossendorff, F.A. Schildberg, Articular cartilage regeneration and tissue engineering models: a systematic review, Arch. Orthop. Trauma Surg. 139 (2019) 305–316, doi:10.1007/s00402-018-3057-z.

[22] J. Fu, P. He, D.-A. Wang, Articular cartilage tissue engineering, in: A. Hasan (Ed.), Tissue Engineering for Artificial Organs: Regenerative Medicine, Smart Diagnostics and Personalized Medicine, 1, Wiley Online Library, 2017, pp. 243–295, doi:10.1002/9783527689934.ch8.

[23] E.Y. Salinas, J.C. Hu, K.A. Athanasiou, A guide for using mechanical stimulation to enhance tissue-engineered articular cartilage properties, Tissue Eng. Part B Rev. 24 (2018) 345–358, doi:10.1089/ten.teb.2018.0006.

[24] H. Jahr, C. Matta, A. Mobasheri, Physicochemical and biomechanical stimuli in cell-based articular cartilage repair, Curr. Rheumatol. Rep. 17 (2015) 22, doi:10.1007/s11926-014-0493-9.

[25] M.A. Brady, S.D. Waldman, C.R. Ethier, The application of multiple biophysical cues to engineer functional neo-cartilage for treatment of osteoarthritis. Part I: cellular response, Tissue Eng. Part B Rev. 21 (2015) 1–19, doi:10.1089/ten.teb.2013.0757.

[26] M.A. Brady, S.D. Waldman, C.R. Ethier, The application of multiple biophysical cues to engineer functional neocartilage for treatment of osteoarthritis. Part II: signal transduction, Tissue Eng. Part B Rev. 21 (2015) 20–33, doi:10.1089/ten.teb.2013.0760.

[27] K. Iwasa, A.H. Reddi, Pulsed electromagnetic fields and tissue engineering of the joints, Tissue Eng. Part B Rev. 24 (2018) 144–154, doi:10.1089/ten.teb.2017.0294.

[28] A.R. Farooqi, J. Zimmermann, R. Bader, U. van Rienen, Numerical simulation of electroactive hydrogels for cartilage – tissue engineering, Materials (Basel). 12 (2019) 2913, doi:10.3390/ma12182913.

[29] A.R. Farooqi, R. Bader, U. van Rienen, Numerical study on electromechanics in cartilage tissue with respect to its electrical properties, Tissue Eng. Part B Rev. 25 (2019) 152–166, doi:10.1089/ten.teb.2018.0214.

[30] J.J. Vaca-González, J.F. Escobar, J.M. Guevara, Y.A. Hata, G. Gallego Ferrer, D.A. Garzón-Alvarado, Capacitively coupled electrical stimulation of rat chondroepiphysis explants: A histomorphometric analysis, Bioelectrochemistry 126 (2019) 1–11, doi:10.1016/j.bioelechem.2018.11.004.

[31] Z. Ji, K. Yan, W. Li, H. Hu, X. Zhu, Mathematical and computational modeling in complex biological systems, Biomed Res. Int. 2017 (2017) 5958321, doi:10.1155/2017/5958321.

[32] S.L. Peck, Simulation as experiment: a philosophical reassessment for biological modeling, Trends Ecol. Evol. 19 (2004) 530–534, doi:10.1016/j.tree.2004.07.019.

[33] J.W. Holmes, Model first and ask questions later: confessions of a reformed experimentalist, J. Biomech. Eng. 141 (2019) 074701, doi:10.1115/1.4043432.

[34] L. Geris, et al., Computational Modeling in Tissue Engineering, Springer, Berlin, Heidelberg, 2013, doi:10.1007/978-3-642-32563-2.

[35] E.G. Baylon, M.E. Levenston, Osmotic swelling responses are conserved across cartilaginous tissues with varied sulfated-glycosaminoglycan contents, J. Orthop. Res. 38 (2020) 785–792, doi:10.1002/jor.24521.

[36] M. Lv, Y. Zhou, X. Chen, L. Han, L. Wang, X.L. Lu, Calcium signaling of in situ chondrocytes in articular cartilage under compressive loading: roles of calcium sources and cell membrane ion channels, J. Orthop. Res. 36 (2018) 730–738, doi:10.1002/jor.23768.

[37] Y. Zhou, M.A. David, X. Chen, L.Q. Wan, R.L. Duncan, L. Wang, X.L. Lu, Effects of osmolarity on the spontaneous calcium signaling of in situ juvenile and adult articular chondrocytes, Ann. Biomed. Eng. 44 (2016) 1138–1147, doi:10.1007/s10439-015-1406-4.

[38] A. Mobasheri, C. Matta, I. Uzielienè, E. Budd, P. Martín-Vasallo, E. Bernotiene, The chondrocyte channelome: a narrative review, Jt. Bone Spine 86 (2019) 29–35, doi:10.1016/j.jbspin.2018.01.012.

[39] B. Tandon, A. Magaz, R. Balint, J.J. Blaker, S.H. Cartmell, Electroactive biomaterials: Vehicles for controlled delivery of therapeutic agents for drug delivery and tissue regeneration, Adv. Drug Deliv. Rev. 129 (2018) 148–168, doi:10.1016/j.addr.2017.12.012.

[40] C. Ning, Z. Zhou, G. Tan, Y. Zhu, C. Mao, Electroactive polymers for tissue regeneration: developments and perspectives, Prog. Polym. Sci. 81 (2018) 144–162, doi:10.1016/j.progpolymsci.2018.01.001.

[41] H. Kwon, W.E. Brown, C.A. Lee, D. Wang, N. Paschos, J.C. Hu, K.A. Athanasiou, Surgical and tissue engineering strategies for articular cartilage and meniscus repair, Nat. Rev. Rheumatol. 15 (2019) 550–570, doi:10.1038/s41584-019-0255-1.

[42] E.A. Makris, A.H. Gomoll, K.N. Malizos, J.C. Hu, K.A. Athanasiou, Repair and tissue engineering techniques for articular cartilage, Nat. Rev. Rheumatol. 11 (2015) 21–34, doi:10.1038/nrrheum.2014.157.

[43] X. Huang, R. Das, A. Patel, T. Duc Nguyen, Physical stimulations for bone and cartilage regeneration, Regen. Eng. Transl. Med. 4 (2018) 216–237, doi:10.1007/s40883-018-0064-0.

[44] N. More, G. Kapusetti, Piezoelectric material - a promising approach for bone and cartilage regeneration, Med. Hypotheses 108 (2017) 10–16, doi:10.1016/j.mehy.2017.07.021.

[45] H.J. Kwon, Tissue engineering of muscles and cartilages using polyelectrolyte hydrogels, Adv. Mater. Sci. Eng. 2014 (2014) 154071, doi:10.1155/2014/154071.

[46] N. Eslahi, M. Abdorahim, A. Simchi, Smart polymeric hydrogels for cartilage tissue engineering: a review on the chemistry and biological functions, Biomacromolecules 17 (2016) 3441–3463, doi:10.1021/acs.biomac.6b01235.

[47] S. Ansari, S. Khorshidi, A. Karkhaneh, Engineering of gradient osteochondral tissue: from nature to lab, Acta Biomater. 87 (2019) 41–54, doi:10.1016/j.actbio.2019.01.071.

[48] T. Gonzalez-Fernandez, P. Sikorski, J.K. Leach, Bio-instructive materials for musculoskeletal regeneration, Acta Biomater. 96 (2019) 20–34, doi:10.1016/j.actbio.2019.07.014.

[49] J. Xu, W. Wang, C.C. Clark, C.T. Brighton, Signal transduction in electrically stimulated articular chondrocytes involves translocation of extracellular calcium through voltage-gated channels, Osteoarthr. Cartil. 17 (2009) 397–405, doi:10.1016/j.joca.2008.07.001.

[50] J. Jacob, N. More, K. Kalia, G. Kapusetti, Piezoelectric smart biomaterials for bone and cartilage tissue engineering, Inflamm. Regen. 38 (2018) 2, doi:10.1186/s41232-018-0059-8.

[51] M. Doi, M. Matsumoto, Y. Hirose, Deformation of ionic polymer gels by electric fields, Macromolecules 25 (1992) 5504–5511, doi:10.1021/ma00046a058.

[52] T. Shiga, T. Kurauchi, Deformation of polyelectrolyte gels under the influence of electric field, J. Appl. Polym. Sci. 39 (1990) 2305–2320, doi:10.1002/app.1990.070391110.

[53] T. Shiga, Deformation and viscoelastic behavior of polymer gels in electric fields, in: Neutron spin echo Spectrosc. viscoelasticity Rheol., Springer, 1997, pp. 131–163, doi:10.1007/3-540-68449-2_2.

[54] P.J. Flory, J. Rehner, Statistical mechanics of cross-linked polymer networks I. Rubberlike elasticity, J. Chem. Phys. 11 (1943) 512–520, doi:10.1063/1.1723792.

[55] P.J. Flory, J. Rehner, Statistical mechanics of cross-linked polymer networks II. Swelling, J. Chem. Phys. 11 (1943) 521–526, doi:10.1063/1.1723792.

[56] P.J. Flory, Principles of Polymer Chemistry, Cornell University Press, Ithaca, New York, NY, USA, 1953.

[57] F.G. Donnan, The theory of membrane equilibria, Chem. Rev. 1 (1924) 73–90, doi:10.1021/cr60001a003.

[58] P.E. Grimshaw, J.H. Nussbaum, A.J. Grodzinsky, M.L. Yarmush, Kinetics of electrically and chemically induced swelling in polyelectrolyte gels, J. Chem. Phys. 93 (1990) 4462–4472, doi:10.1063/1.458729.

[59] P.E. Grimshaw, A.J. Grodzinsky, M.L. Yarmush, D.M. Yarmush, Dynamic membranes for protein transport: chemical and electrical control, Chem. Eng. Sci. 44 (1989) 827–840, doi:10.1016/0009-2509(89)85256-X.

[60] V.C. Mow, S.C. Kuei, W.M. Lai, C.G. Armstrong, Biphasic creep and stress relaxation of articular cartilage in compression: theory and experiments, J. Biomech. Eng. 102 (1980) 73–84, doi:10.1115/1.3138202.

[61] W.M. Lai, J.S. Hou, V.C. Mow, A triphasic theory for the swelling and deformation behaviors of articular cartilage, J. Biomech. Eng. 113 (1991) 245–258, doi:10.1115/1.2894880.

[62] J.M. Huyghe, J.D. Janssen, Quadriphasic mechanics of swelling incompressible porous media, Int. J. Eng. Sci. 35 (1997) 793–802, doi:10.1016/S0020-7225(96)00119-X.

[63] W.Y. Gu, W.M. Lai, V.C. Mow, A mixture theory for charged-hydrated soft tissues containing multi-electrolytes: passive transport and swelling behaviors, J. Biomech. Eng. 120 (1998) 169–180, doi:10.1115/1.2798299.

[64] W.Y. Gu, W.M. Lai, V.C. Mow, Transport of multi-electrolytes in charged hydrated biological soft tissues, Transp. Porous Media 34 (1999) 143–157, doi:10.1023/A:1006561408186.

[65] W.Y. Gu, W.M. Lai, V.C. Mow, Theoretical basis for measurements of cartilage fixed-charge density using streaming current and electro-osmosis effects, in: Proc. 1993 ASME Winter Annu. Meet. New Orleans, LA, USA, 1993, pp. 55–58.

[66] X. Zhou, Y.C. Hon, S. Sun, A.F.T. Mak, Numerical simulation of the steady-state deformation of a smart hydrogel under an external electric field, Smart Mater. Struct. 11 (2002) 459–467, doi:10.1088/0964-1726/11/3/316.

[67] Y.C. Hon, M.W. Lu, A.F.T. Mak, X. Zhou, Mechano-electrochemical response analysis of a hydrogel strip under electric field, in: Adv. Comput. Eng. Sci., Tch Science Press, 2000, pp. 1681–1686.

[68] H. Li, Z. Yuan, K.Y. Lam, H.P. Lee, J. Chen, J. Hanes, J. Fu, Model development and numerical simulation of electric-stimulus-responsive hydrogels subject to an externally applied electric field, Biosens. Bioelectron. 19 (2004) 1097–1107, doi:10.1016/j.bios.2003.10.004.

[69] H. Li, J. Chen, K.Y. Lam, Multiphysical modeling and meshless simulation of electric-sensitive hydrogels, J. Polym. Sci. Part B Polym. Phys. 42 (2004) 1514–1531, doi:10.1002/polb.20025.

[70] T. Wallmersperger, B. Kröplin, R.W. Gülch, Coupled chemo-electro-mechanical formulation for ionic polymer gels - numerical and experimental investigations, Mech. Mater. 36 (2004) 411–420, doi:10.1016/S0167-6636(03)00068-1.

[71] T. Wallmersperger, B. Kröplin, J. Holdenried, R.W. Gülch, A coupled multi-field-formulation for ionic polymer gels in electric fields, in: SPIE's 8th Annu. Int. Symp. Smart Struct. Mater., 2001, pp. 264–275, doi:10.1117/12.432655.

[72] H.P. Langtangen, K.-A. Mardal, Introduction to numerical methods for variational problems, Texts in Computational Science and Engineering, 1, Springer International Publishing, Switzerland, 2019, doi:10.1007/978-3-030-23788-2.

[73] F. Helfferich, Ion Exchange, McGraw-Hill Book Company, Inc., New York, NY, USA, 1962.

[74] , Solid State Electrochemistry, P.G. Bruce (Ed.), Cambridge University Press, Cambridge, UK, 1995, doi:10.1017/CBO9780511524790.

[75] W. Nernst, Zur Kinetik der in Lösung befindlichen Körper, Zeitschrift für Phys. Chemie 2U (1888) 613–637, doi:10.1515/zpch-1888-0274.

[76] W. Nernst, Die elektromotorische Wirksamkeit der Jonen, Zeitschrift für Phys. Chemie 4U (1889) 129–181, doi:10.1515/zpch-1889-0412.

[77] M. Planck, Ueber die Erregung von Electricität und Wärme in Electrolyten, Ann. Phys. 275 (1890) 161–186, doi:10.1002/andp.18902750202.

[78] F. Brezzi, M. Fortin, Mixed and hybrid finite element methods, volume 15 of Springer Series in Computational Mathematics, Springer-Verlag, 1991, doi:10.1007/978-1-4612-3172-1.

[79] M.G. Larson, F. Bengzon, The finite element method: theory, implementation, and applications, 10, Springer Science & Business Media, 2013, doi:10.1007/978-3-642-33287-6.

[80] M.S. Gockenbach, Understanding and Implementing the Finite Element Method, Society for Industrial and Applied Mathematics, Philadelphia, PA, USA, 2006, doi:10.1137/1.9780898717846.

[81] A. Logg, K.-A. Mardal, G.N. Wells, Automated Solution of Differential Equations by the Finite Element method_The FEniCS Book, Springer-Verlag, Berlin, Heidelberg, 2012, doi:10.1007/978-3-642-23099-8.

[82] P. Amestoy, I.S. Duff, J.-Y. L'Excellent, J. Koster, A fully asynchronous multifunctional solver using distributed dynamic scheduling, SIAM J. Matrix Anal. Appl. 23 (2001) 15–41, doi:10.1137/S0895479899358194.

[83] D.S. Chandrasekharaiah, L. Debnath, Continuum Mechanics, Academic Press, San Diego, 1994, doi:10.1016/C2009-0-21209-8.

[84] T. Tanaka, L.O. Hocker, G.B. Benedek, Spectrum of Light Scattered from a Viscoelastic Gel, J. Chem. Phys. 59 (1973) 5151–5159, doi:10.1063/1.1680734.

[85] F. Horkay, I. Tasaki, P.J. Basser, Osmotic Swelling of Polyacrylate Hydrogels in Physiological Salt Solutions, Biomacromolecules 1 (2000) 84–90, doi:10.1021/bm9905031.

[86] M.A. Biot, Theory of deformation of a porous viscoelastic anisotropic solid, J. Appl. Phys. 27 (1956) 459–467, doi:10.1063/1.1722402.

[87] H. Li, J. Chen, K.Y. Lam, Transient simulation of kinetics of electric-sensitive hydrogels, Biosens. Bioelectron. 22 (2007) 1633–1641, doi:10.1016/j.bios.2006.07.016.

[88] H. Li, Kinetics of smart hydrogels responding to electric field: a transient deformation analysis, Int. J. Solids Struct. 46 (2009) 1326–1333, doi:10.1016/j.ijsolstr.2008.11.001.

[89] C. Yu, K. Malakpoor, J.M. Huyghe, A three-dimensional transient mixed hybrid finite element model for superabsorbent polymers with strain-dependent permeability, Soft. Matter 14 (2018) 3834–3848, doi:10.1039/c7sm01587a.

[90] P.J. Basser, A.J. Grodzinsky, The Donnan model derived from microstructure, Biophys. Chem. 46 (1993) 57–68, doi:10.1016/0301-4622(93)87007-J.

[91] M.D. Buschmann, A.J. Grodzinsky, A molecular model of proteoglycan-associated electrostatic forces in cartilage mechanics, J. Biomech. Eng. 117 (1995) 179–192, doi:10.1115/1.2796000.

[92] J.T.G. Overbeek, The donnan equilibrium, Prog. Biophys. Biophys. Chem. 6 (1956) 57–84, doi:10.1016/S0096-4174(18)30104-5.

[93] R.W. Gülch, J. Holdenried, A. Weible, T. Wallmersperger, B. Kröplin, Polyelectrolyte gels in electric fields: a theoretical and experimental approach, in: Proc. SPIE 3987, Smart Struct. Mater. 2000 Electroact. Polym. Actuators Devices, 3987, 2000, pp. 193–202, doi:10.1117/12.387778.

[94] J.J. Vaca-González, J.M. Guevara, M.A. Moncayo, H. Castro-Abril, Y.A. Hata, D.A. Garzón-Alvarado, Biophysical stimuli: a review of electrical and mechanical stimulation in Hyaline cartilage, Cartilage 10 (2019) 157–172, doi:10.1177/1947603517730637.

[95] T. Ning, K. Zhang, B.C. Heng, Z. Ge, Diverse effects of pulsed electrical stimulation on cells - with a focus on chondrocyte and cartilage regeneration, Eur. Cells Mater. 38 (2019) 79–93, doi:10.22203/eCM.v038a07.

[96] T. Wallmersperger, D. Ballhause, Coupled chemo-electro-mechanical finite element simulation of hydrogels: II. Electrical stimulation, Smart Mater. Struct. 17 (2008) 1–10, doi:10.1088/0964-1726/17/4/045012.

[97] A.H. Doulabi, K. Mequanint, H. Mohammadi, Blends and nanocomposite biomaterials for articular cartilage tissue engineering, Materials (Basel). 7 (2014) 5327–5355, doi:10.3390/ma7075327.

[98] C. Madeira, A. Santhagunam, J.B. Salgueiro, J. Cabral, Advanced cell therapies for articular cartilage regeneration, Trends Biotechnol. 33 (2015) 35–42, doi:10.1016/j.tibtech.2014.11.003.

[99] T. Ning, J. Guo, K. Zhang, K. Li, J. Zhang, Z. Yang, Z. Ge, Nanosecond pulsed electric fields enhanced chondrogenic potential of mesenchymal stem cells via JNK/CREB-STAT3 signaling pathway, Stem Cell Res. Ther. 10 (2019) 45, doi:10.1186/s13287-019-1133-0.

[100] J.J. Vaca-González, S. Clara-Trujillo, M. Guillot-Ferriols, J. Ródenas-Rochina, M.J. Sanchis, J.L.G. Ribelles, D.A. Garzón-Alvarado, G.G. Ferrer, Effect of electrical stimulation on chondrogenic differentiation of mesenchymal stem cells cultured in hyaluronic acid - Gelatin injectable hydrogels, Bioelectrochemistry 134 (2020) 107536, doi:10.1016/j.bioelechem.2020.107536.

[101] M. Ganser, F.E. Hildebrand, M. Kamlah, R.M. McMeeking, A finite strain electro-chemo-mechanical theory for ion transport with application to binary solid electrolytes, J. Mech. Phys. Solids 125 (2019) 681–713, doi:10.1016/j.jmps.2019.01.004.

[102] G. Pattappa, J. Zellner, B. Johnstone, D. Docheva, P. Angele, Cells under pressure - the relationship between hydrostatic pressure and mesenchymal stem cell chondrogenesis, Eur. Cells Mater. 37 (2019) 360–381, doi:10.22203/eCM.v037a22.

[103] H.L. Lim, J.C. Chuang, T. Tran, A. Aung, G. Arya, S. Varghese, Dynamic electromechanical hydrogel matrices for stem cell culture, Adv. Funct. Mater. 21 (2011) 55–63, doi:10.1002/adfm.201001519.

[104] P.W. Hsieh, S.Y. Yang, A new stabilized linear finite element method for solving reaction-convection-diffusion equations, Comput. Methods Appl. Mech. Eng. 307 (2016) 362–382, doi:10.1016/j.cma.2016.04.024.

[105] D. Pearce, S. Fischer, F. Huda, A. Vahdati, Applications of computer modeling and simulation in cartilage tissue engineering, Tissue Eng. Regen. Med. 17 (2019) 1–13, doi:10.1007/s13770-019-00216-9.

[106] S. Krüeger, S. Achilles, J. Zimmermann, T. Tischer, R. Bader, A. Jonitz-Heincke, Re-differentiation capacity of human chondrocytes in vitro following electrical stimulation with capacitively coupled fields, J. Clin. Med. 8 (2019) 1771, doi:10.3390/jcm8111771.

[107] T. Distler, F. Ruther, A.R. Boccaccini, R. Detsch, Development of 3D biofabricated cell Laden hydrogel vessels and a low-cost desktop printed perfusion chamber for in vitro vessel maturation, Macromol. Biosci. 19 (2019) 1900245, doi:10.1002/mabi.201900245.

[108] T. Distler, A.R. Boccaccini, 3D printing of electrically conductive hydrogels for tissue engineering and biosensors - A review, Acta Biomater. 101 (2020) 1–13, doi:10.1016/j.actbio.2019.08.044.